Bulletin of the Geological Survey of Japan, vol. 52 (9), p. 405–423, 2001

Characterizing fracture systems of Kyushu, southwest Japan through satellite-image derived lineaments superimposed on topographic and lithologic data

Katsuaki KOIKE[1], Ryoichi KOUDA[2] and Toshiaki UEKI[3]

Katsuaki KOIKE, Ryoichi KOUDA and Toshiaki UEKI (2001) Characterizing fracture systems of Kyushu, southwest Japan through satellite-image derived lineaments superimposed on topographic and lithologic data. *Bull. Geol. Surv. Japan,* vol. 52 (9), p. 405–423, 17 figs.

Abstract: Lineament analysis targeting both the land and the sea floor is important for comprehensive understanding of local and regional fracture systems, because some of the major lineaments are related to fracture zones that can emplace mineral and geothermal resources. For this reason, we have developed an automatic extraction method of lineaments, the Segment Tracing Algorithm (STA), and a vector-analysis technique to calculate azimuths and dips of interpreted fractures through the combination of lineament data and digital elevation model (DEM) data. The Kyushu district, southwest Japan, is chosen as a study area and 77,893 lineaments are derived from the three full-scene LANDSAT TM band 4 images of the district. For the rich epithermal gold deposits, it is illustrated that the azimuths of the continuous fractures estimated near the deposits correspond generally to those of the principal veins. This correlation suggests an angular relationship between directional emplacement of the gold deposits and the tectonics that produced the fractures oriented in the estimated directions. For the geothermal field in the middle Kyushu, the significant fractures which act as conduits for transport of hydrothermal fluids to the ground surface can be identified. In addition, a lineament analysis for the sea floor is conducted using the shaded DEM of 1 km mesh, produced by interpolating the sea-depth data. A combination of lineament maps of the land and the sea floor is useful to identify tectonically significant lineaments that are continuous over the two regions and consider a genetic mechanism of the fracture systems.

1. Introduction

Understanding spatial distribution of rock fractures is significant to various fields in geosciences, including tectonics for paleo and present stress field, hydrogeology for fracture-affected flow channels, rock mechanics for displacement behavior and maintainability of rock masses, and resource exploration for vein-type mineral deposits and fluids in fractured reservoirs (e.g., Rowan and Wetlaufer, 1981; Rouleau and Gale, 1985; National Research Council, 1996; Coward *et al.,* 1998; Adler and Thovert, 1999). We use here "fracture" as general term of geologic discontinuity that involves fault, joint, and fissure. Although sizes of fractures range from micro- to macro-scales, dominant directions of the fractures, which were formed under a regional stress field, are in some cases common to all the scales (Engelder, 1982). Therefore, dominant directions can provide information useful in the above fields.

It is difficult to clarify the dominant directions and spatial distribution of fractures from investigation data limited in both quantity and location. The most extensive method for fracture characterization is remote sensing of land surface by aerophotographs and satellite images. This method is based on the fact that the largely damaged portions tend to be selectively eroded and formed as continuous valleys. When these valleys are illuminated by electro-magnetic waves at inclined angles, conspicuous linear features, "lineaments", appear on both optical and microwave sensor images. Due to weathering and vegetation in humid and warm areas such as Japan, much information on fractures is concealed in remotely sensed images. However, the dominant directions of continuous fractures with wide fracture zones can be distinguished from lineament distribution, which requires a suitable method for precisely extracting lineaments. From this view point, Koike *et al.* (1995) developed a

[1] Faculty of Engineering, Kumamoto University. Kurokami 2–39–1, Kumamoto, 860–8555 Japan
[2] Geoinformation Division, GSJ
[3] Ocean High Technology Institute Inc. Honcho 2–51–10, Nakano-ku, Tokyo, 164–0012 Japan

Keywords : LANDSAT TM image, lineament analysis, digital elevation model, fracture, sea floor, Kyushu

Segment Tracing Algorithm (STA) as an automatic extraction method of lineaments.

Another point should be noted that fractures are three-dimensionally extending planes represented by strikes and dips. It is necessary, for lineament analysis aimed at clarification of subsurface geologic structures, to construct fracture planes and to estimate their strikes and dips. Koike *et al.* (1998) developed a new method to calculate azimuths and dips of interpreted fractures through the combination of lineament data and digital elevation models (DEMs). A vector-analysis technique is used in this method.

In this paper, the STA and the estimation method of fracture orientation are applied to Kyushu district, southwest Japan. Kyushu is known to be dominated by geothermal and mineral resources because of containing volcanic belts, but also suffers from natural disasters such as earthquake and debris flow. This feature is closely associated with the existence of fracture systems ranging over various scales. Kyushu has a special tectonic environment which is under an extensional stress field. To detect local and regional characteristics of fracture systems in Kyushu, we used LANDSAT TM images, DEMs, surficial geological map, and shaded images of bathymetry and examined directional features of the interpreted fracture planes.

2. Automatic Lineament Extraction and Estimating Fracture Planes

The STA is a nonfiltering approach to the accurate extraction of a continuous straight valley. Briefly, it detects a line element (segment) which identifies a lineament by the following five steps.

[step 1] Local window with array size of 11 by 11 pixels is set around a centered pixel which will be judged on whether it is a line element (Fig. 1). The 16 directions at 11.25° intervals passing through the center of the window are defined to examine a local variation of gray levels along a line. Numbers in Figure 1 denote examples of the line directions. The direction which minimizes the variation is assumed to be the valley direction and expressed by a symbol k_{min}.

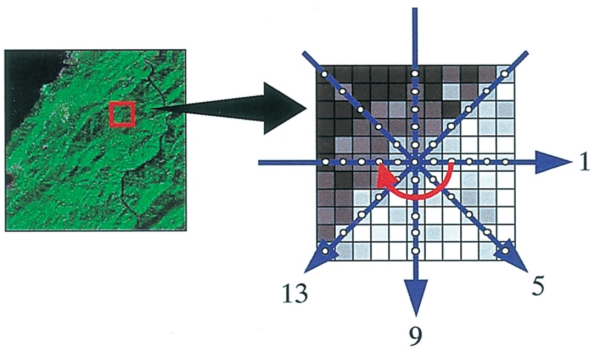

Fig. 1 Local window with array size of 11 by 11 pixels and scan lines at $\pi/16$ radian intervals used in the Segment Tracing Algorithm. Numbers denote examples of line directions for examining a local variation of gray levels.

[step 2] Let a gray level at location x by $z(x)$. Along the direction perpendicular to k_{min}, that is k_{max}, squared secondary differentiation for gray levels, λ, is calculated.

$$\lambda = \left\{ \frac{d^2 z(x)}{dx^2} \right\}^2 \Big/ z(x) \qquad (1)$$

Expressing the mean and the standard deviation of the λ by m and σ, a dynamic threshold, T, is defined as :

$$T = m + \mu\sigma, \quad \mu = \phi_1 / [1 + (\eta - 1)\sin\theta] \qquad (2)$$

where θ is the included angle between the sun's azimuth (s_p) and k_{max}, and ϕ_1 is a constant (=2). The line elements which lie in the closer direction of s_p have a lower threshold level. If the value calculated at the centered pixel of the window is above the threshold, the pixel is retained as a line element (p).

The η is a parameter introduced to consider an image texture that is expressed by spatial autocorrelation of gray levels. Let the semivariograms for the gray levels along the s_p and the direction perpendicular to it (s_c) be γ_p and γ_c, respectively. Semivariogram expresses relation between distance of data pair and variance of it (e.g., David, 1977). Using the γ_p and γ_c calculated by the gray-level pairs at adjacent two pixels, we define the value of η as the γ_p divided by γ_c.

[step 3] Judging whether the p represents a ridge or valley feature is performed and the p assumed to be distributed at a ridge is eliminated.

[step 4] This routine is to link the derived line elements. The distance between p and the connectable pixels are examined within the distance H from p :

$$H = \phi_2 / [1 + (\eta - 1)\cos\theta] + \phi_3 \qquad (3)$$

where ϕ_2 and ϕ_3 are constants with values of 4 and 8, respectively. The value H also is a dynamic threshold such that two pixels lying parallel to s_p and having a larger distance can be linked.

[step 5] A center line for the line elements, which have similar directions and intersect each other, is obtained from the (x, y) coordinates of the line elements using principal component analysis.

More details on the STA are described in Koike *et al.* (1995, 1999). The STA has been proved to applicable to a couple of sensor images and various areas in Japan, but lineaments extracted by the STA are shorter, in most cases, than faults described by geological maps and individual faults usually consist of several disconnected lineaments. Such situations are due to discontinuous changes of gray levels and the limited area of image analyzed at a single time. Accordingly, several lineaments that are considered to belong to the same fracture system can be connected based on the criterion of distance and similarity of directional

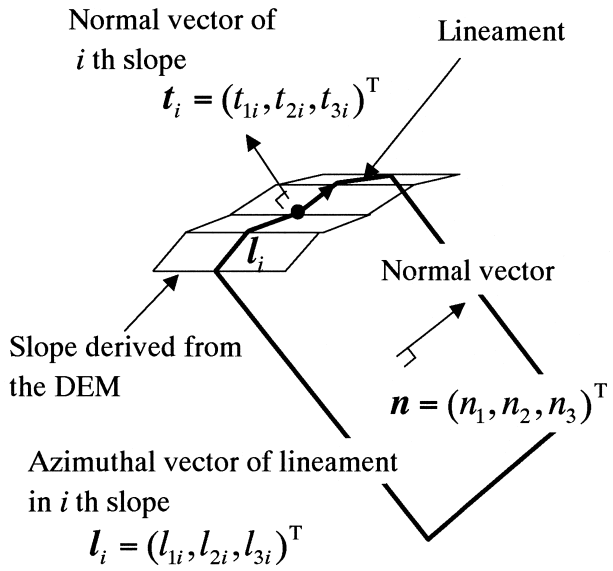

Fig. 2 Definition of vectors used in the estimation method of azimuth of interpreted fracture plane.

angle.

Next step is estimating azimuth of concatenated lineaments. The principle of this method proposed by Koike *et al.* (1998) founds on that the appearance pattern of fractures on the terrain depends on their dip angles. This geometrical relationship can be described through vector analysis. According to the assumption of fracture shape being a plane with finite dimensions, we express a normal vector of a plane, $\boldsymbol{n}$. A slope is made by the DEM and its normal vector is represented by $\boldsymbol{t}_i$ ($i=1, 2, \cdots, m_s$), where m_s is the number of slopes through which the lineaments classified into the same group pass. Let the azimuthal vector of the lineament be $\boldsymbol{l}_i$. The $\boldsymbol{l}_i$ is equivalent to the intersection of the desired plane and the slope i (Fig. 2). Therefore, the $\boldsymbol{l}_i$ should be equal to the vector product of two normal vectors :

$$\boldsymbol{l}_i = \boldsymbol{t}_i \times \boldsymbol{n} \quad (i=1, 2, \cdots, m_s) \tag{4}$$

Obviously, $\boldsymbol{n}$ is the only unknown in this equation. It is prudent, therefore, to obtain $\boldsymbol{n}$ by applying the least-squares method and solving the normal equation that is deduced from :

$$\frac{\partial}{\partial \boldsymbol{n}} \left\{ \sum_{i=1}^{m_s} \omega_i (\boldsymbol{l}_i - \boldsymbol{t}_i \times \boldsymbol{n})^T (\boldsymbol{l}_i - \boldsymbol{t}_i \times \boldsymbol{n}) \right\} = 0 \tag{5}$$

where ω_i is a weighting coefficient and T means transposition of a vector. Furthermore, directional relationship between $\boldsymbol{n}$ and the average vector of $\boldsymbol{t}_i$ is used to judge whether the obtained plane represents a normal fault or reverse fault feature (Koike *et al.*, 1999).

3. Estimation and Characterization of Local Fracture System from Lineaments

3.1 Results of Extraction and Grouping of Lineaments over the Study Area

Three full-scene images of LANDSAT TM, which mostly cover Kyushu as shown in Figure 3, were used for the lineament analysis. Acquisition dates and (path-row) of the images for the northeastern, northwestern, and southern parts of Kyushu are March 5, 1993 and (112–37) ; January 18 , 1991 and (113–37) ; and October 22, 1984 and (112–38), respectively. Figure 3 is a false-color composite image with band 2 as blue, 3 as red, and 4 as green. Because reflectance of surface material varies with wavelength, the lineament analysis requires to discover the imagery from multi-band data whose gray levels correspond to characteristics of topography. Gray levels of LANDSAT TM band 4 correlate well with the reflectance of shaded-relief images derived from a DEM of forested area of Japan (Koike *et al.*, 1995). Therefore, band-4 data were used.

From the area shown in Figure 3, 77,893 lineaments were extracted through the STA and these were classified into 16,694 groups. The η in Eqs. (2) and (3) was defined as 1.5. The lineament extraction was executed for the area covering 36 km×36 km (1,200×1,200 pixels) at one time, whose up-and-down and right-and-left 6 km portions are overlapped the neighboring images in order to prevent from disrupting a continuous lineament, and the extraction was repeated for all the divided images. Figure 3 includes an example of lineament distribution extracted from a unit area. Some advantages of the STA are found by its capability to extract more lineaments that parallel the sun's azimuth (the northwest) and those located in shadow areas.

Each lineament was projected on the DEM of 250 m mesh and the digital geological map, G-1, at a scale of 1 : 1,000,000 (Geological Survey of Japan, 1995) using affine transformation with first-order polynomial. Figure 4 shows distribution of lineaments classified into groups longer than 5 km and overlaid with the DEM. To demonstrate in detail the result of grouping, a unit area located eastward the Hitoyoshi basin is enlarged in Figure 4. The numbers of groups that could be judged as normal fault type and reverse fault type are 2,090 and 3,238, respectively. From pole-density distributions using the lower hemisphere projection of Schmidt's net (Fig. 5), dominancy of the northeast trending planes constructed from the lineaments is found in common to both the fault types, but dip directions are different. Southward dips and northward dips are distinguished in the normal and reverse fault types, respectively. Another feature is that the ratio of northwest trending planes to the northeast trending ones is larger in the normal fault type.

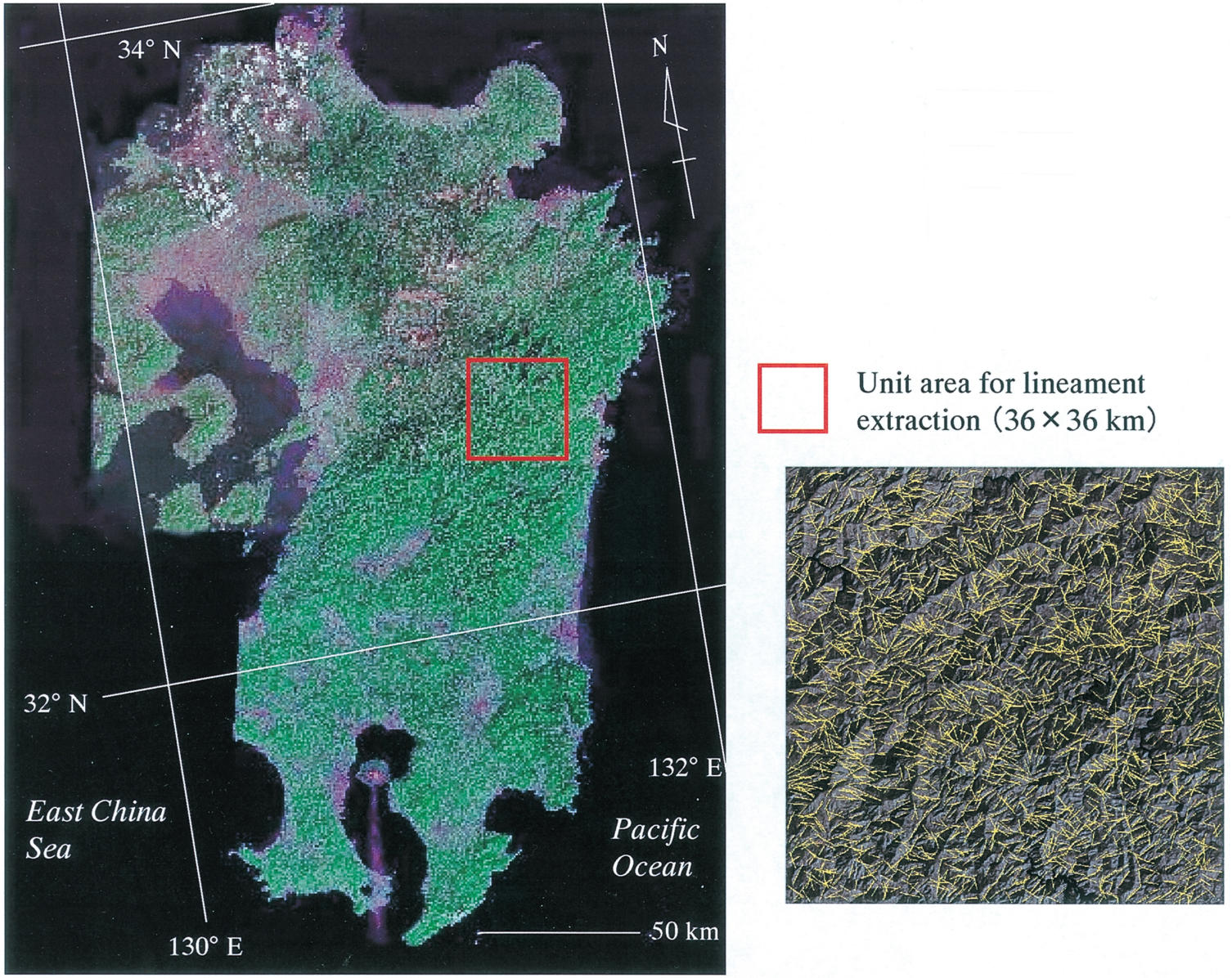

Fig. 3 Landsat TM false-color composite image of Kyushu district, southwest Japan and an example of lineament distribution extracted from unit area by the STA.

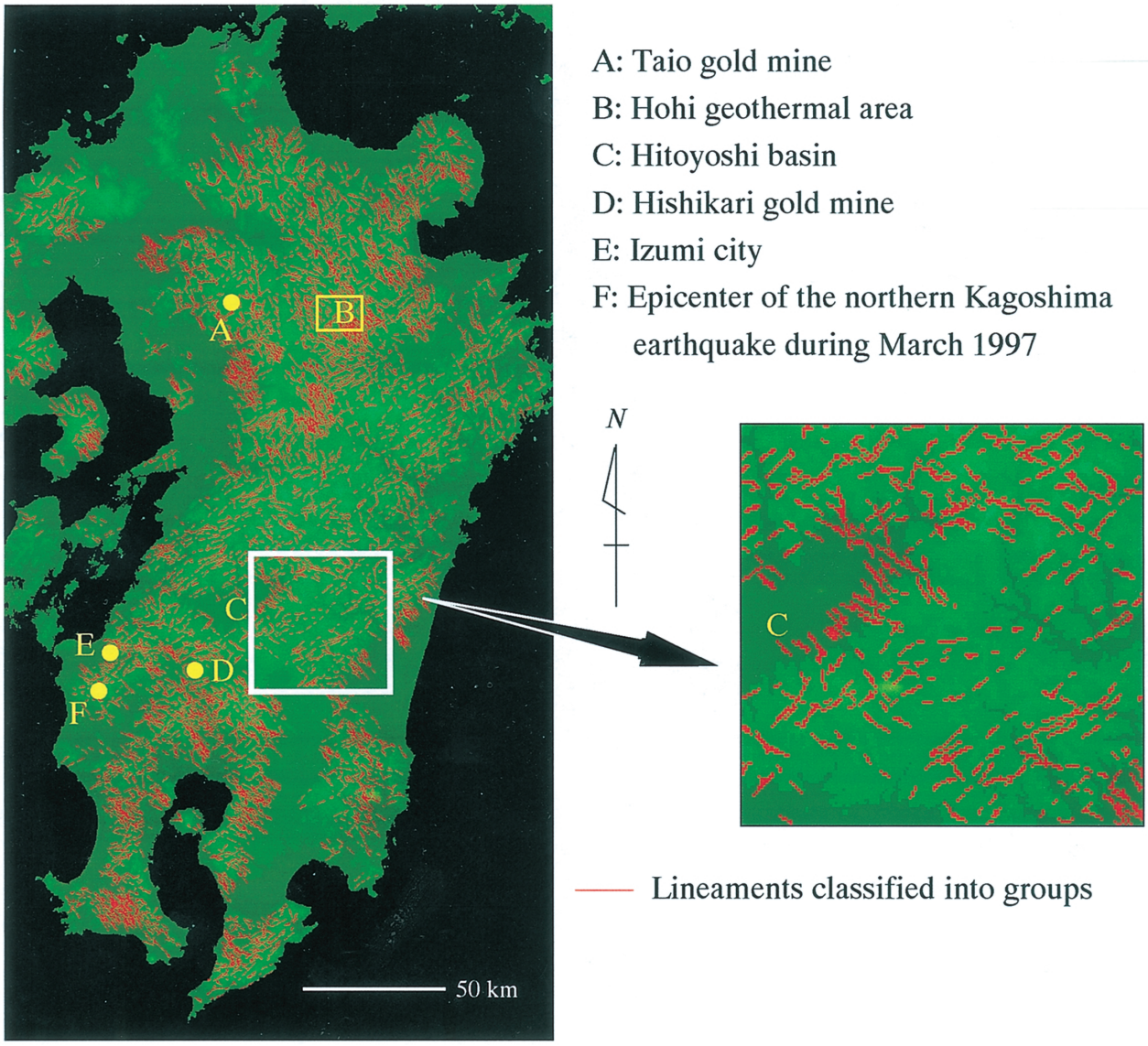

Fig. 4 Distribution of lineaments classified into groups longer than 5 km and overlaid with digital elevation model of 250 m mesh.

3.2 Azimuthal Correlation between Estimated Fractures and Veins

The Hishikari mine, located in the northern Kagoshima prefecture, southern Kyushu (Fig. 4) is known to be a typical epithermal vein-type deposit and one of the richest gold mine in Japan. High grade potions are accumulated in the veins, composed of mainly quartz and adularia, which intrude into the Shimanto supergroup of Cretaceous age and Kakuto volcanic rocks of Quaternary age. Average strike and dip of the main veins with 0.5–1 m wide are reported to be N60°E and 80°NW (MMIJ, 1989). Figure 6 shows the lineaments extracted near the Hishikari mine and pole direction of the twenty fracture planes estimated from these lineaments. Numbers in Figure 6 denote examples of the groups into which several lineaments are classified and their corresponding pole directions. Average strike of the twenty planes is N63°E and 70% of them dip northwestward with an average dip angle of 83°. Therefore, close azimuthal correlation between the continuous fractures estimated near the mine and the principal veins can be noted for the Hishikari mine. This correlation suggests an angular relationship between directional emplacement of the gold deposits and the tectonics that produced the fractures oriented in the estimated directions. The mine is located at gravity-high anomaly zone with a northeast-southwest axis, which suggests the vein systems occurred at the crest of Shimanto supergroup, basement rocks in this area (Urashima *et al.*, 1987).

Similar angular correlation between the fractures estimated from satellite-derived lineaments and veins was clarified in the Taio gold mine area, northern Kyushu (Fig. 4) by Koike *et al.* (1998). In this area, the

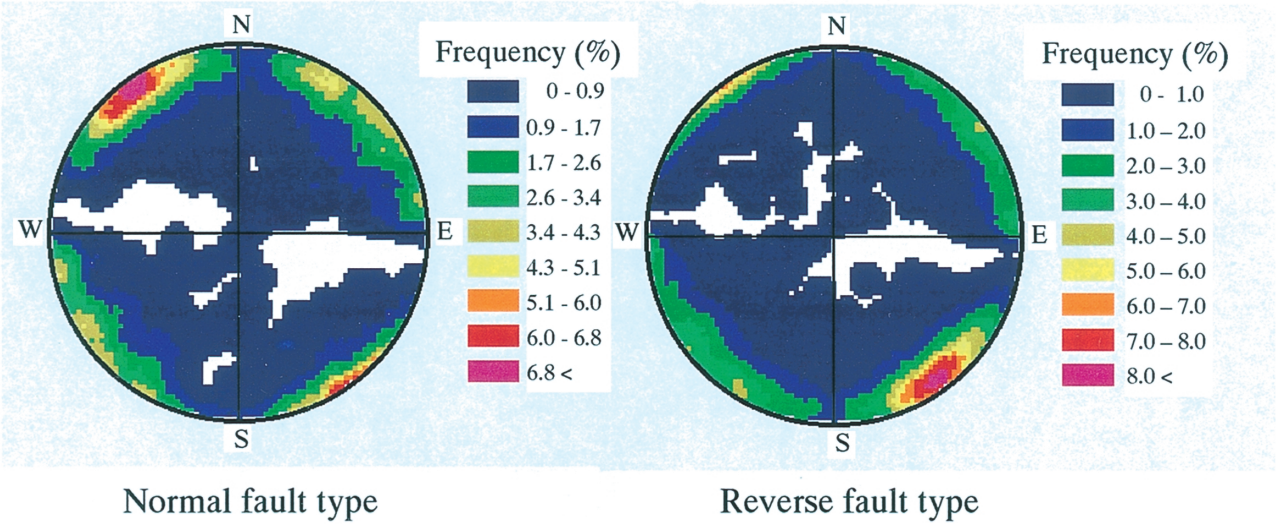

Fig. 5 Azimuthal frequencies of estimated fracture planes of normal fault type and reverse fault type using the lower hemisphere projection of the Schmidt's net.

dominant directions of the estimated fractures are northwest and west-northwest. Another comparative study for fracture systems over different scales was carried out for the Kamaishi mine area, northeastern Japan, where an Early Cretaceous dioritic granite (partly by diorite) batholith outcrops (Koike *et al.*, 1998). It was found that the predominant joint direction, observed in the drifts, corresponds to the direction of the most continuous fracture plane, whose trace length is larger than 10 km. From these results, an existence of the self-similarity concerning the azimuthal distribution of fractures is detected in several areas with different rock types and geologic ages. This confirms that dominant directions of satellite-derived lineaments are important to mineral exploration and rock engineering because they can be extrapolated into small scale fractures.

3.3 Fracture Distribution Near Epicenter

Earthquake activity was remarkable during 1997 in the northern Kagoshima prefecture. The strongest earthquake during March 1997 with an intensity of 6.3 on the Richter scale hit the area. Its epicenter is shown in Figure 4. The earthquake has a characteristic in that it is centered in the shallow depth of about 8 km. Based on the focal mechanism and the aftershocks distributed along the east-west direction with 15 km long, left lateral slip movement of a fault plane trending the east-west is considered to be a cause for the earthquake. In this area, active faults striking northeast, termed Izumi fault system, are known (The Research Group for Active Tectonics in Kyushu, 1989). Figure 7 shows the lineaments extracted in the area. From these lineaments, two sets of fracture planes which generally strike N50°E and N60°W and dip 70°NW and 75°NE, respectively, were estimated. The former set corresponds to the strike and location of Izumi fault system and the latter set is chiefly distributed near the epicenter. These estimated fractures appear to form a conjugate fracture system under a regional compressive stress field. The strike of the latter set ranges from N40°W to N70°W and the axis of aftershock distribution trends about N80°W. Although these directions do not agree with each other, one of the west-northwest fault planes, which has conjugate relation to the Izumi fault system, may have left-laterally slipped. This assumed fault plane is latent because lineaments striking N80°W are not extracted near the epicenter.

3.4 Fracture Distribution in Debris Flow Area

Large debris flows occurred in Izumi city, Kagoshima prefecture (Fig. 4) during July 1997 followed by the slope failures. In this area, many lineaments trending northeast, which correspond to the strike of Minamata-Minami fault system, were extracted as shown in Figure 8. At the damaged area, two kinds of rock masses, which are both composed of andesite but distinguished by the degree of weathering, are distributed in contact with each other. This boundary cannot be judged as a fault plane, but an existence of fault is estimated near the boundary (Nakazawa, 1997). The lineaments distributed near the damaged area construct a plane that strikes N55°E and dips 88°NW. Though the dip is almost vertical, dip direction of the estimated fracture plane corresponds to the one of slopes, which means the plane is regarded as normal fault type. The plane may be one factor causing the slope failures.

3.5 Fracture Configuration and Hydrothermal Flow in Geothermal Area

The Hohi geothermal area, situated near the prefecture boundary between Oita and Kumamoto in north-

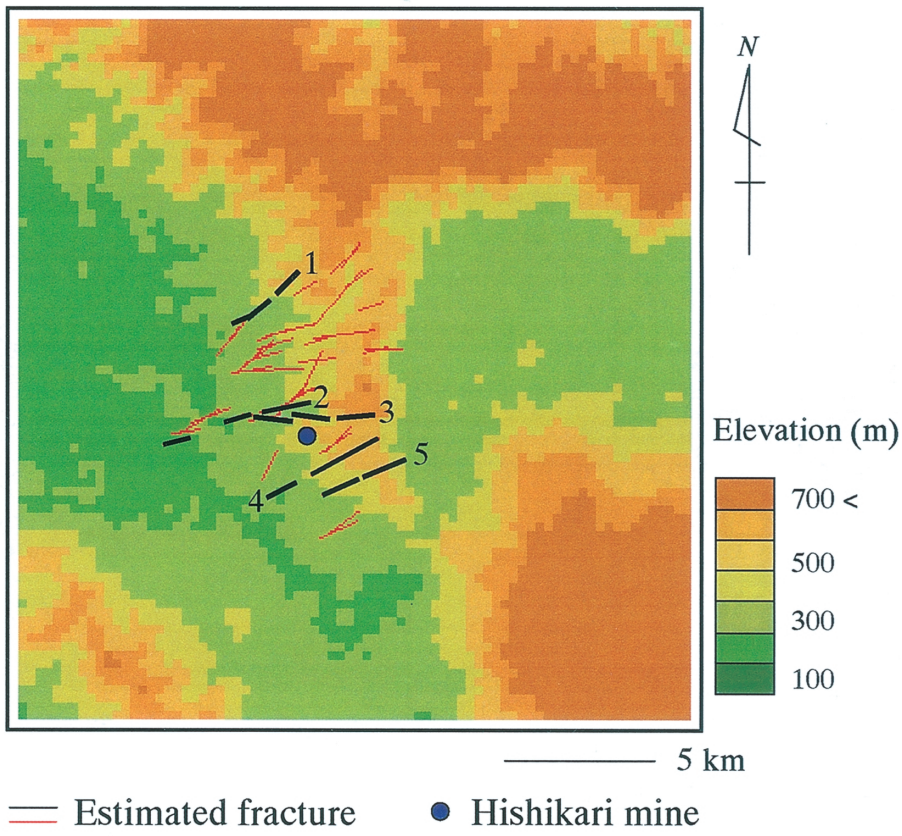

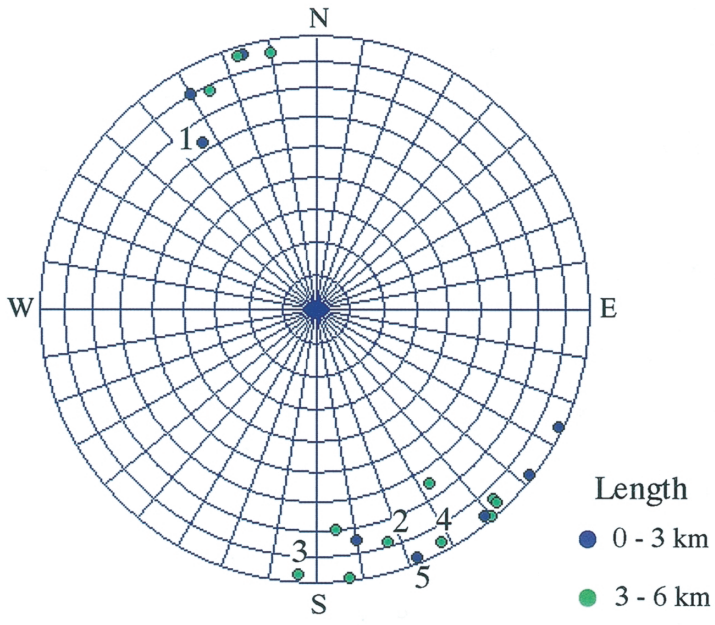

Fig. 6 Lineaments extracted near the Hishikari gold mine and pole direction of the twenty fracture planes estimated from the lineaments. Numbers denote examples of the groups into which several lineaments are classified and their corresponding pole directions.

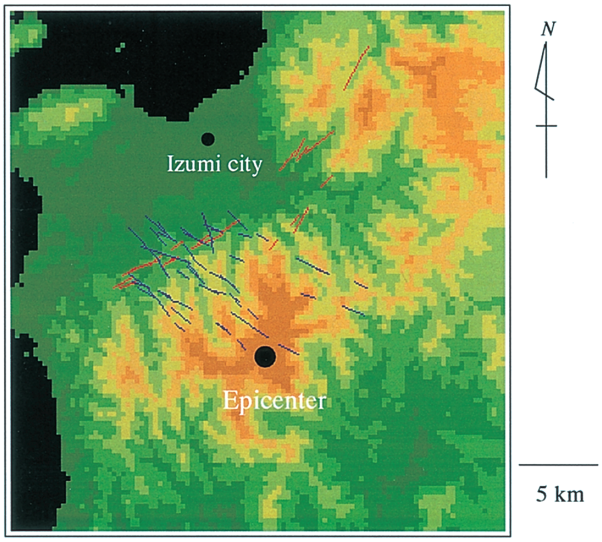

Fig. 7 Lineaments around the epicenter occurred during March 1997 in the northern Kagoshima prefecture, which show a conjugate fracture system.

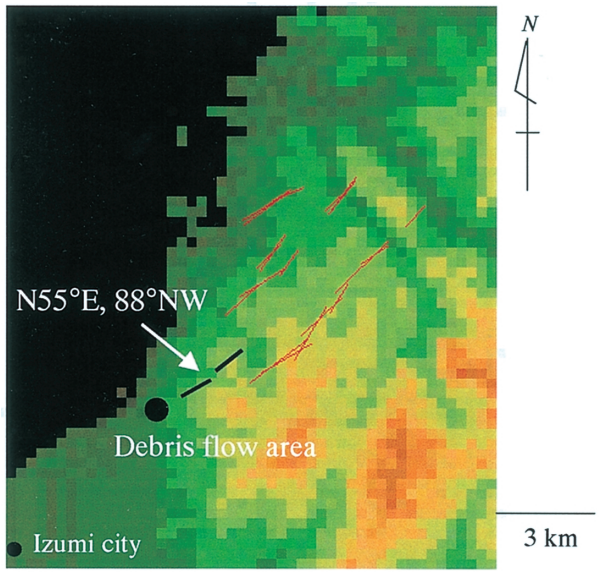

Fig. 8 Lineaments around the large debris flow area occurred during July 1997 in Izumi city, northern Kagoshima prefecture.

ern Kyushu (Fig. 4) is well known to be rich in geothermal resources because it contains several hot springs, two actual geothermal power stations, and active volcanoes. Fractures are believed to act as conduits for transporting hydrothermal fluids and also as geothermal reservoirs in this area.

Figure 9(a) illustrates a perspective view of distribution of fracture planes longer than 5 km estimated from the extracted lineaments. The dominant directions of these planes are north-northwest and northwest, and the east-northeast is subordinate to them. These northwest trending planes seem to be connected to form fracture zones passing through the hot springs and geothermal manifestations on the ground. The Otake and Hatchobaru power stations are located near the intersection of estimated fracture zones. A fracture plane constructed near the Takenoyu hot spring dips northeast and forms reverse fault type. The dip direction corresponds to the one of Takenoyu fault inferred from the correlation of several geologic columns (Tamanyu, 1985).

Such a fracture-system map can be incorporated into a numerical simulation using finite element method for the hydrothermal fluid flow. Taking estimated fracture distribution into account, two large fracture zones, which are considered to have strong effect on the hydrothermal fluid flows, are set as shown in Figure 9(b) and their dips are defined as vertical. We adopted a typical hydrothermal flow analysis and simplified the problem by assuming a single phase flow under the steady state. The governing equation for this case consists of the thermal energy balance and mass balance.

$$\nabla\cdot\left[\frac{\mathbf{K}\rho}{\mu}\cdot(\nabla P-\rho g\nabla Z)\right]+q_m=0$$
$$\nabla\cdot\left[\frac{\mathbf{K}\rho}{\mu}h\cdot(\nabla P-\rho g\nabla Z)\right]$$
$$+\nabla\cdot\left[K_m\left(\frac{\partial T}{\partial h}\right)_P\nabla h\right]+q_h=0 \qquad (6)$$

where ∇, P, g, ρ, μ, $\mathbf{K}$, Z, q_m, q_h, h, K_m, and T denotes vector differential operator, pressure, gravitational acceleration, density, viscosity, permeability, depth, mass flux, heat flux, enthalpy, thermal conductivity, and temperature, respectively. The flow is assumed to follow Darcy's law. Details of the calculation method, finite element model, and geological model are described in Koike *et al.* (2000) and Koike and Tomita (2000). The principal idea of this calculation is based on Lippmann *et al.* (1997), which divides the calculation area into two regimes considering the phase diagram of water to understand the geothermal system down to deeper horizons. Conductive regime is assumed in the deep depths over which temperature ranges from the Curie point to 300℃. This regime is dominated by heat conduction. The temperature of Curie point is known to change with rock type, but we fixed it as 570℃. For the temperature range between 300℃ and surface temperature, convective regime dominated by fluid convection is defined.

Figure 10 shows two cross-sections along the east-west and passing the hot spring and power station site. Although the dips of fracture zones, elevations of topography, and 300℃ planes are almost the same between the two sections, more complicated flow pattern drawing a curve is found around the power station, and descending flows down to the deeper horizons are remarkable in the section B. This feature

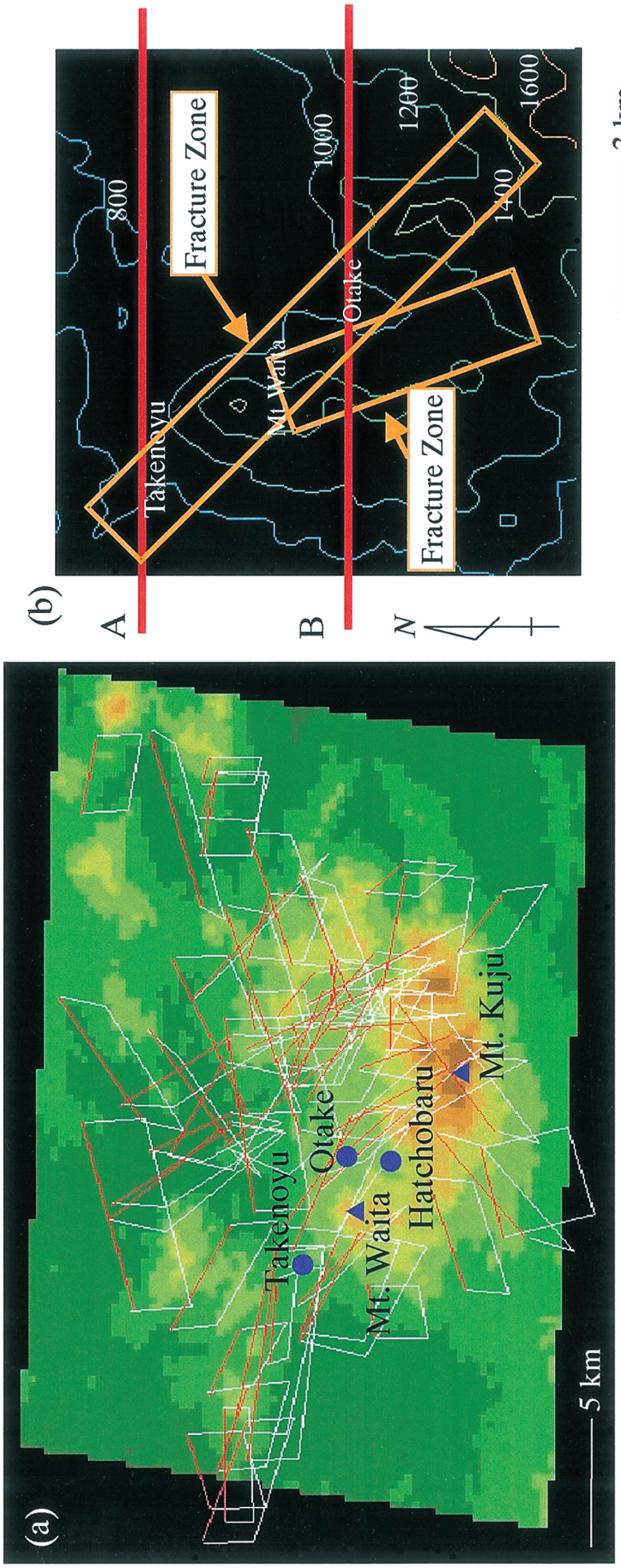

Fig. 9 (a) Perspective view of estimated fracture planes in the Hohi geothermal area and (b) fracture-zone models assumed for a hydrothermal flow analysis. Two lines in (b) indicate location of cross-sections shown in Fig. 10.

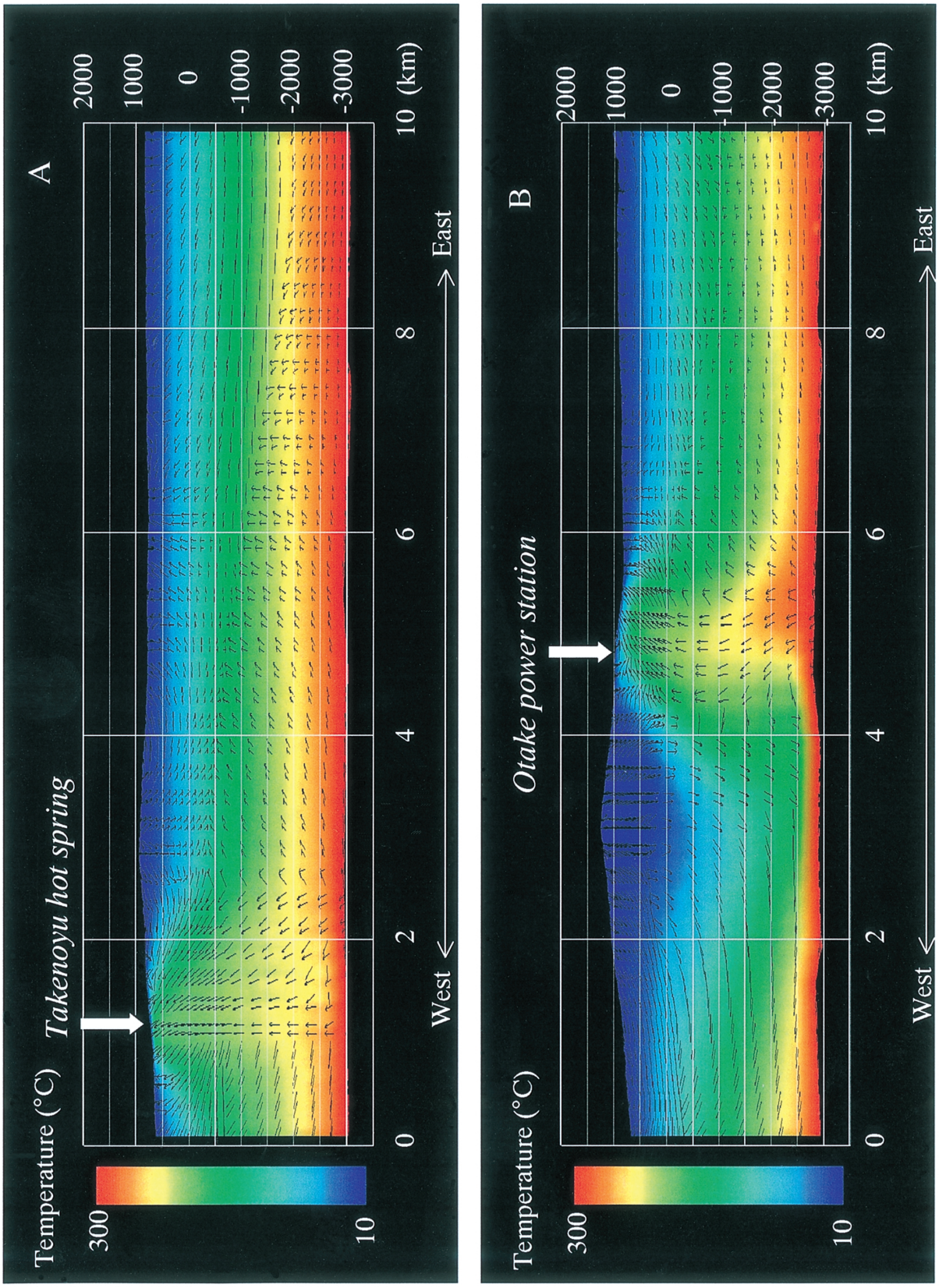

Fig. 10 Cross-sections of temperature distribution and fluid flows estimated from finite element method, along the east-west and passing the hot spring and geothermal power station site.

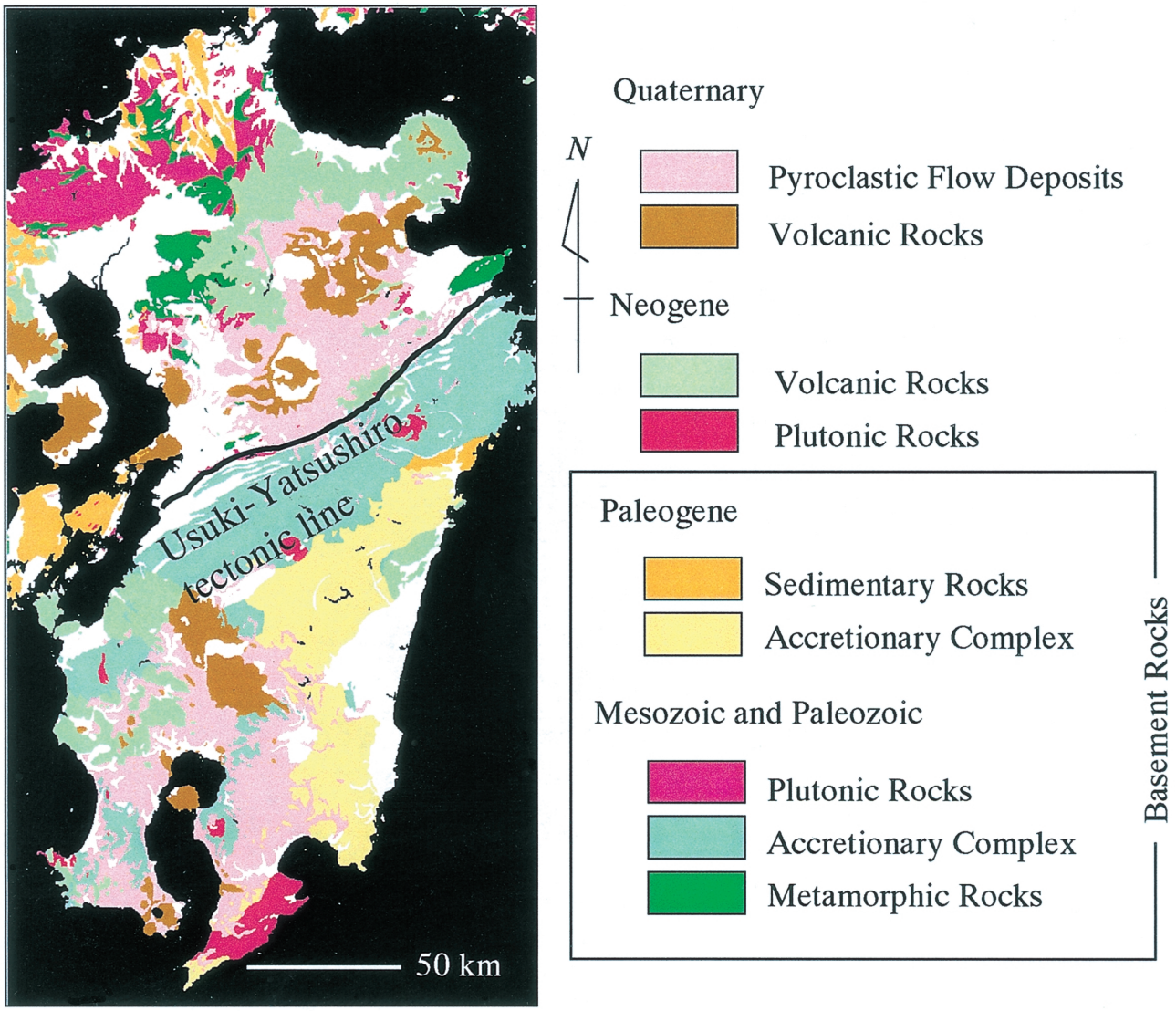

Fig. 11 Digital geological map of Kyushu based on G-1, which was made by combining small lithologic units into a larger rock classification.

may be attributable to the configuration of basement rocks. The top surface of basement rocks are generally shallower than the section A passing through the hot spring.

4. Detection of Azimuthal Distribution Characteristics in Several Lithologic Units

The most distinguished characteristic of Kyushu is that it consists of several east-northeast trending belts with different age and geology. Kyushu is divided into northern and southern parts bordered on the Usuki-Yatsushiro tectonic line (Fig. 11) whose strike agrees with the belts. The northern part is chiefly underlain by the Sangun metamorphic zone and Ryoke zone, while the southern part is chiefly underlain by the Chichibu zone and Shimanto supergroup. These Mesozoic and Paleozoic rocks form the basements of Kyushu. Since there are many active and ancient volcanoes in Kyushu, the Quaternary and Neogene volcanic rocks widely cover the basement rocks. The azimuthal distributions of the fracture planes estimated from the LANDSAT TM image-derived lineaments are arranged from the viewpoint of lithologic unit in which the planes are located.

Figure 11 shows a simplified geological map of Kyushu based on G-1, which was made by combining small lithologic units into a larger rock classification such as sedimentary rocks and volcanic rocks. The main lithologic units of the northern Kyushu is the Mesozoic and Paleozoic metamorphic rocks of the Sangun zone, the Mesozoic plutonic rocks of the Ryoke zone, the Neogene volcanic rocks, and the Quaternary volcanic rocks and pyroclastic flow deposits. We focus on the strike distribution in each lithologic unit as shown in Figure 12. The most remarkable

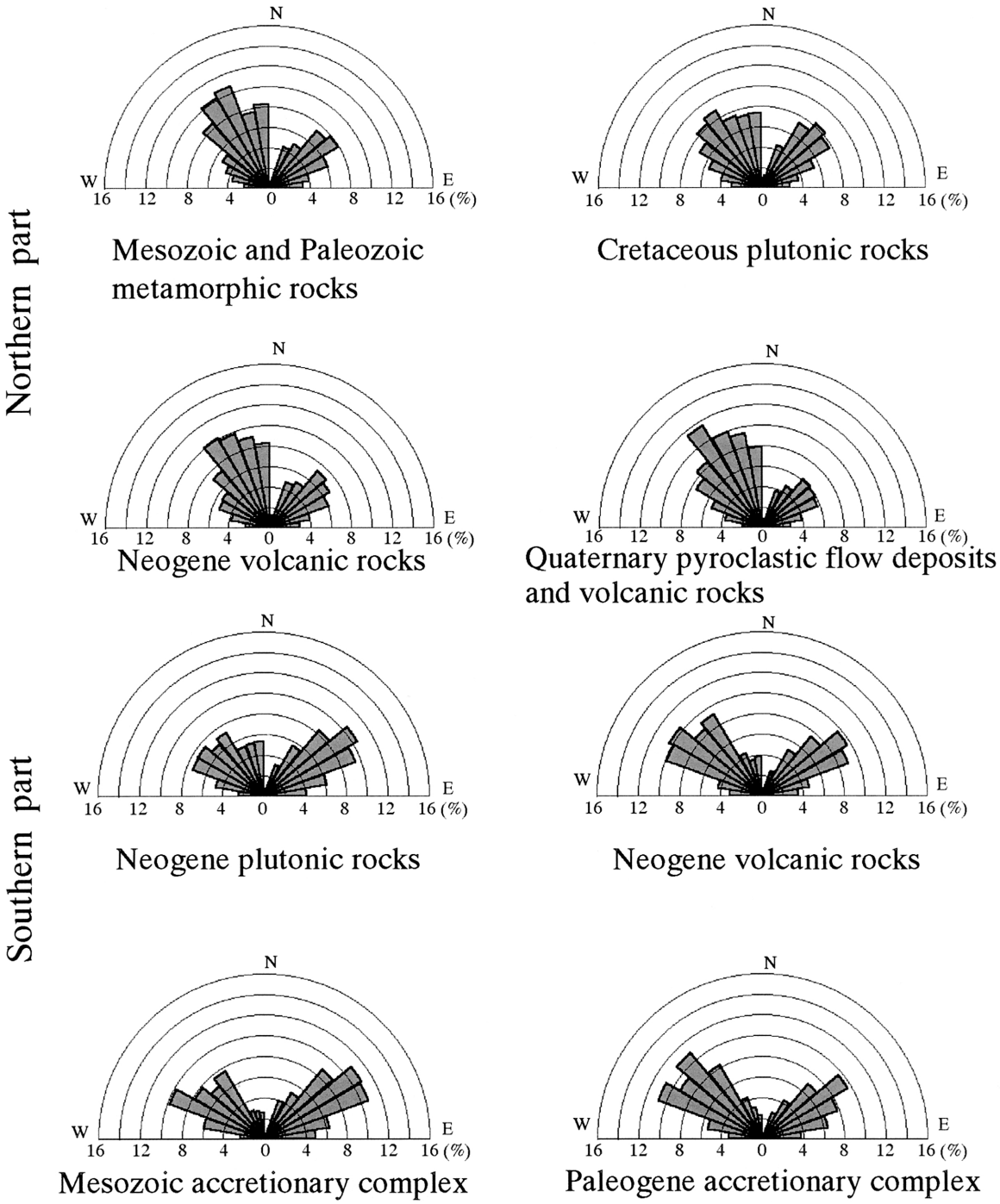

Fig. 12 Comparison of strike frequency of estimated fractures in each lithologic unit between the northern and southern parts of Kyushu.

feature, common to all the lithologic units, is that the northwestward strikes are more noticeable than the northeastward ones and the N40°–50°W take the predominant direction. The frequency of this direction becomes larger inversely with the geologic age. The N10°W is another dominant direction common to the geologic ages. As for the southern Kyushu, the Mesozoic accretionary complex of the Chichibu zone, the Paleogene accretionary complex of the Shimanto supergroup, the Neogene plutonic rocks, and the Neogene volcanic rocks are the main lithologic units. Figure 12 compares the strike distribution of estimated fracture planes in each lithologic unit. It is noteworthy that two sets trending N50°–70°W and N50°–70°E are conspicuous and the frequencies of these directions are roughly the same in all the lithologic units. In the accretionary complex rocks, the northward dipping planes are noticeable than the southward dipping

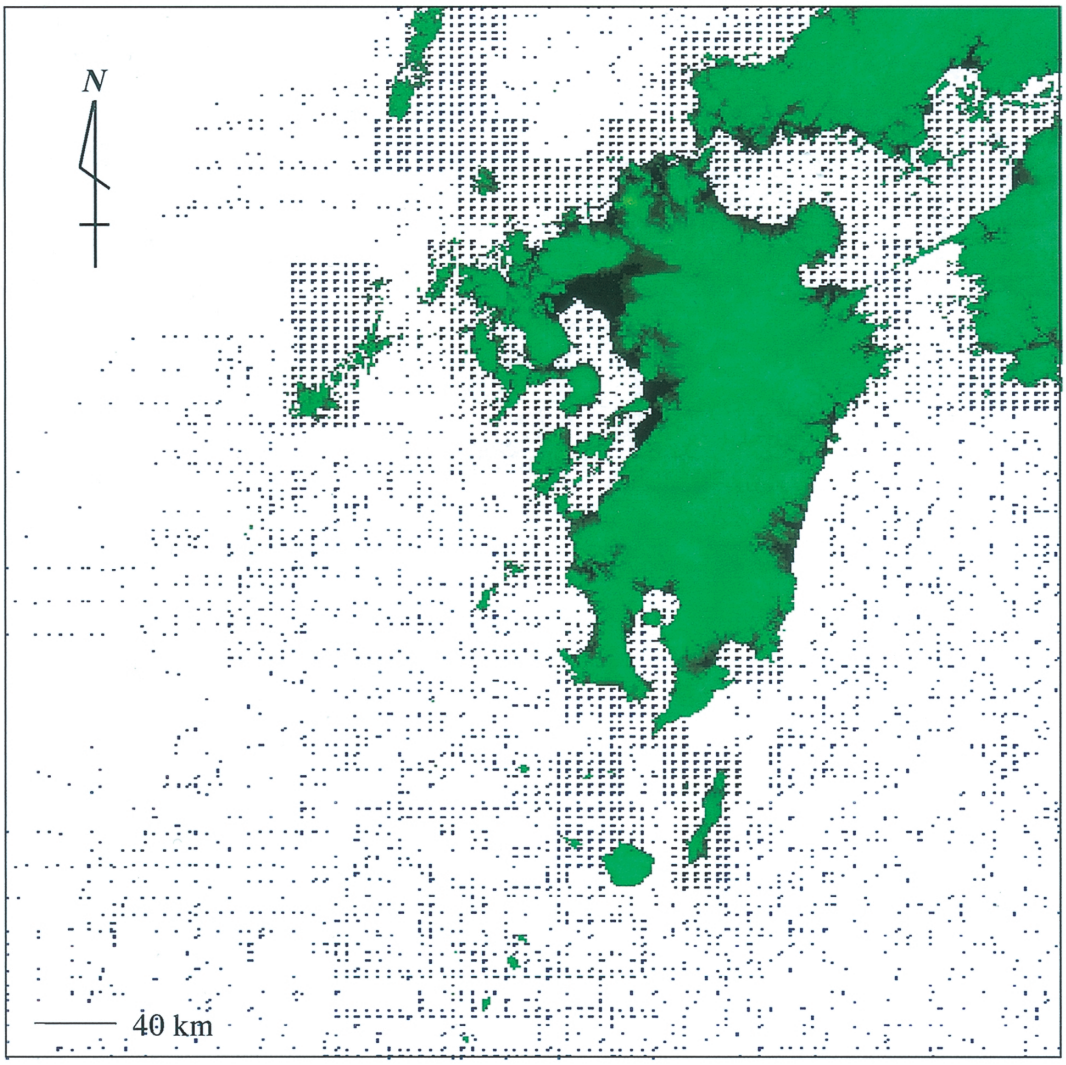

Fig. 13 Distribution of sea-depth data around Kyushu chosen from the Hydrographic Department of Japan (Sea Depth Data in third mesh).

ones, which may indicate imbricate thrust configuration with the accretion.

From these azimuthal frequencies, the fracture-system characteristics in Kyushu are clarified to depend on the geographical difference bounded by the Usuki-Yatsushiro tectonic line rather than the difference of geology. It is considered that an east-west compressive regional stress field have been continued for long time and developed conjugate fracture systems in the southern Kyushu. On the contrary, the strikes in the northern Kyushu are widely distributed. This feature may result from changes of stress fields with geologic age, which implies that the fractures of different formative ages are mixed in the area.

5. Discussion on Regional Fracture System in Kyushu Using Lineaments on Both the Land and Sea Floor

The local characteristics of lineament directions suggests that the north-northwest to northwest lineaments and the northeast to east-northeast lineaments are considered to have tectonic significance in the northern part and southern part of Kyushu, respectively. This is because these directions are noticeable regardless of geologic age and correspond to the directions of active faults. Based on the feature, these trending fractures were probably formed under stress fields of younger geologic ages. In order to consider the genetic mechanism of fractures, the bathymetry around Kyushu is also required to be examined. In general the seafloor surface can show the most recent activity in the Island Arc region so that it is a good example to confirm the assumption. Therefore, lineament analysis targeting both the land and the sea floor is important for comprehensive understanding of regional fracture system and the genetic mechanisms. Bathymetry can be obtained from the processing of sea-depth data.

To construct the bathymetry model around

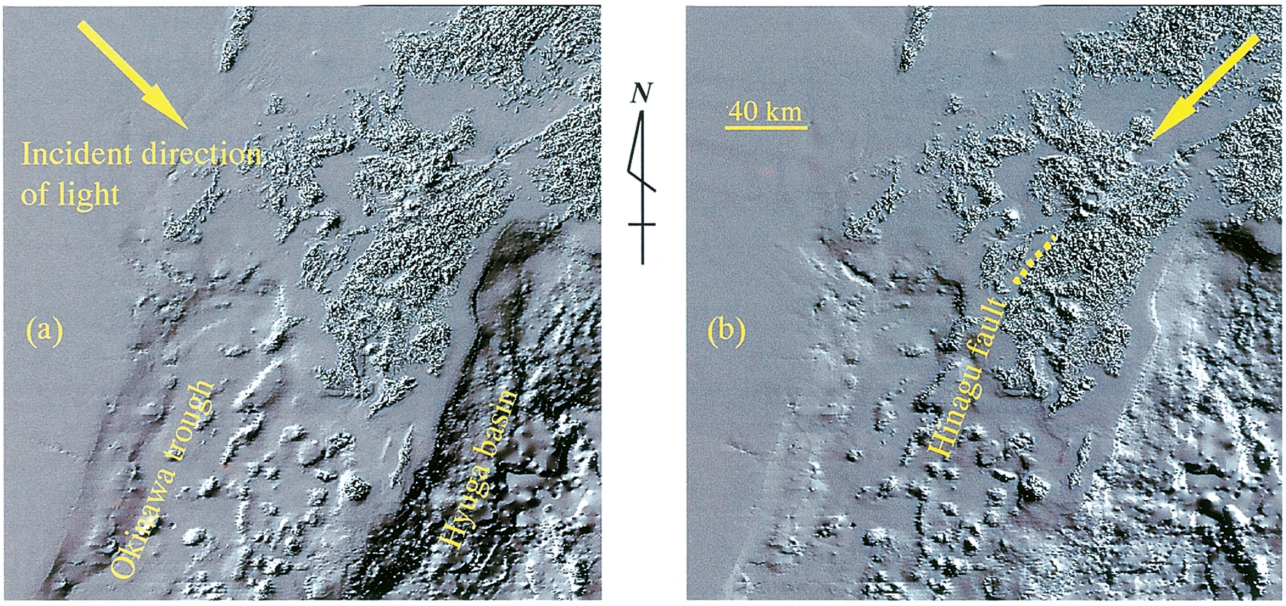

Fig. 14 Shaded relief images based on the constructed bathymetry model. Incident directions of lights are the (a) northwest and (b) northeast.

Kyushu, we used the sea-depth data from the Hydrographic Department of Japan (Sea Depth Data in third mesh) whose spacing is 30″ in the latitude and 45″ in the longitude. The 66,224 data are distributed in the area covering 480 km by 640 km, as shown in Figure 13. Since the data spacings are not uniform, which means the distribution densities vary with location, an interpolation method is necessary to construct a bathymetry model. A method suitable for the spatial variability of data should be selected. The spatial variability is equivalent to semivariogram for a spatial correlation structure. Koike and Ohmi (1999) concluded that a method for making a smooth plane from irregularly spaced data by the minimization criterion of mechanical potential is fitted, because the semivariogram of the sea-depth data illustrated highly correlated feature over wide ranges. For this reason, the two-dimensional optimization principle method proposed by Shiono *et al.* (1987) was adopted.

Shaded relief images through the constructed bathymetry model, illuminated from the northwest and northeast, are depicted in Figure 14. The topographies of the Okinawa trough and Hyuga basin are clearly shown in these figures. Several continuos linear features expressing the existence of active faults on the sea floor are also observed.

The STA was used to extract lineaments from the four shaded relief images illuminated from the west, northwest, north, and northeast. The lineaments from the four images are superimposed on the northwest-illuminated image as shown in Figure 15(a). Due to the lower spatial resolution of the bathymetry model, 1 km mesh, than the LANDSAT TM images, valley features are not sharp and the lineaments do not provide proper information on fracture distribution on the sea floor. Comparing the lineament distribution with the lineaments through the LANDSAT TM images, however, importance of northwest trending and east-northeast trending lines can be confirmed. In special, tectonically significant three lines (A, B, and C), which can be inferred to have continuities over the land and sea floor regions, are drawn in Figure 15(b). Parts of the lines A and B correspond to the Usuki-Yatsushiro tectonic line and Hinagu active fault (Fig. 14), respectively. Figure 16 illustrates the distribution of earthquakes occurred during January 1981 to March 1988 after The Research Group for Active Tectonics in Kyushu (1989). Many earthquakes have occurred along the lines A and B, while earthquakes along the line C are not conspicuous. The active faults in the middle Kyushu trending the northeast have right-lateral slip component. Considering this feature and the distribution characteristic of earthquakes, we propose a hypothesis on the present tectonic model of Kyushu as shown in Figure 17.

Two tectonic movements are regarded as the main cause for configuring the fracture system. One is westward movement of the southern Kyushu accompanied by the compression of the Philippine Sea plate. The other is depression movement at the top of the Okinawa trough. This movement can cause the generation of grabens, represented by the Beppu-Shimabara graben (Fig. 15(b)) in the middle Kyushu ; the earthquake distributions along the lines A and B ; and the development of northwest trending fractures as conjugate fractures in the southern Kyushu, whereas as tensile fractures made with the depression in the northern Kyushu (the earthquakes along the line C

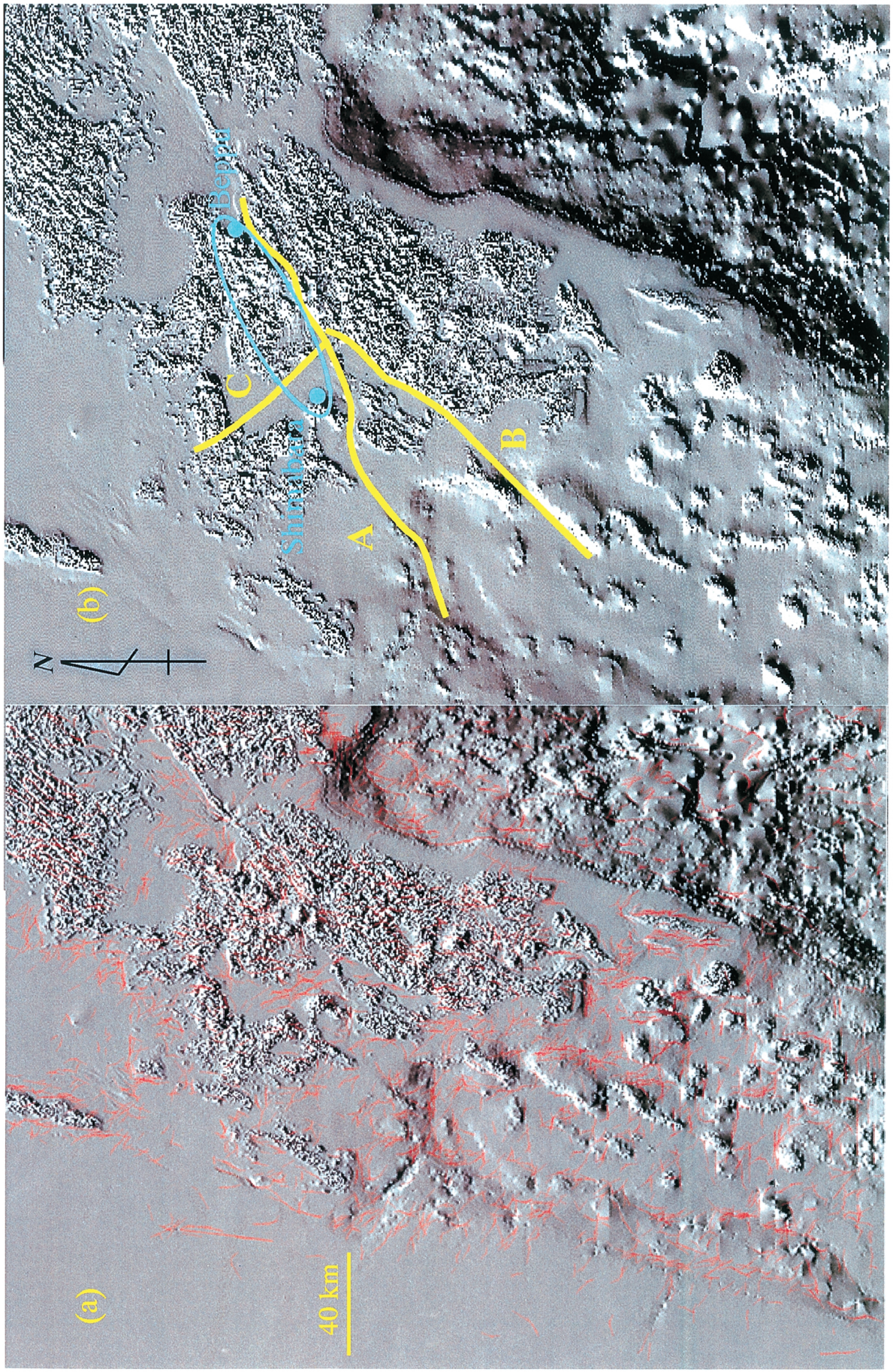

Fig. 15 (a) Lineaments extracted from the bathymetry model by the STA, and (b) three long lines (A, B, and C) estimated to be continuous over the land and sea floor regions and have tectonic significance. Ellipse indicates outline of the Beppu-Shimabara graben.

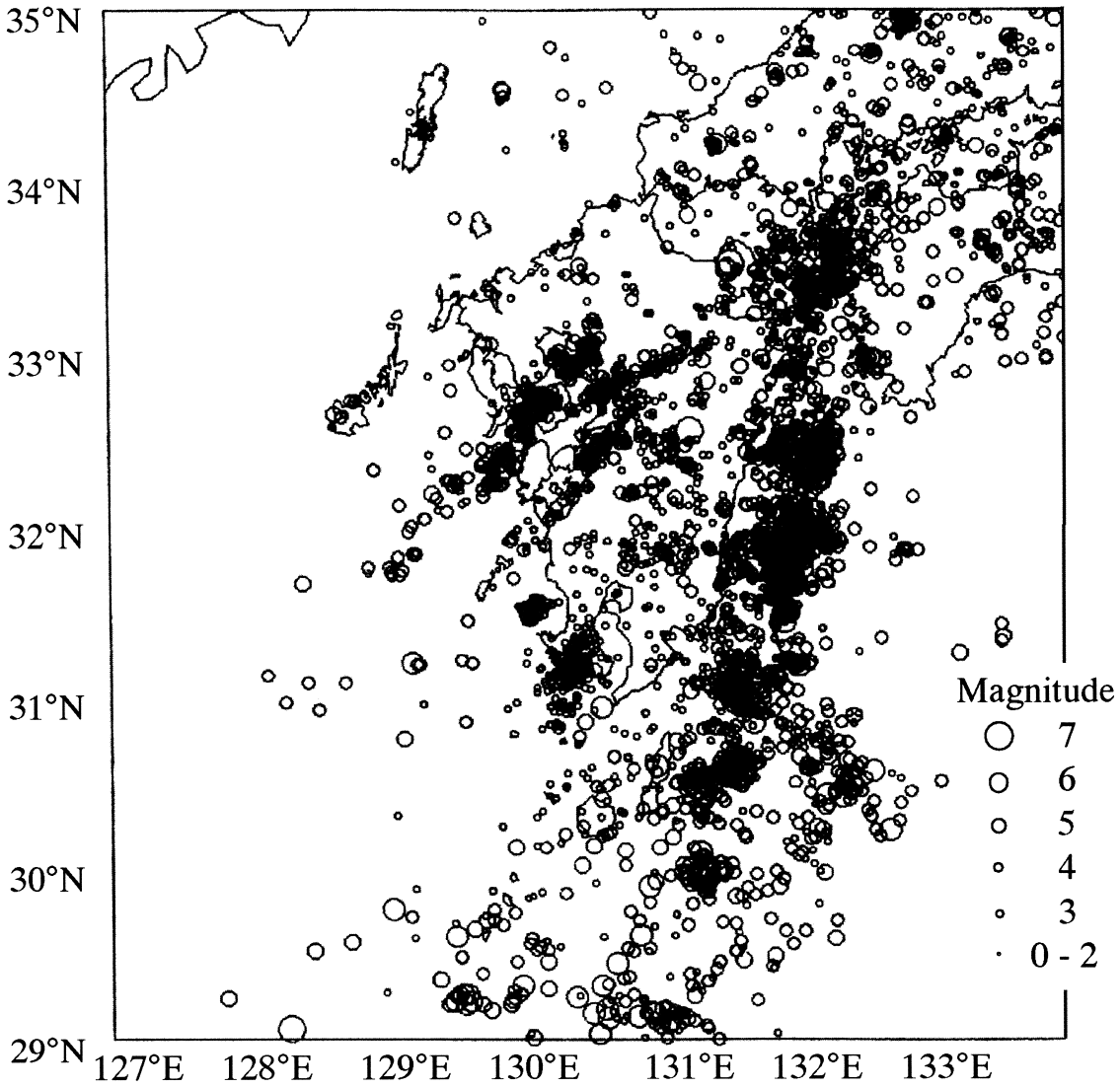

Fig. 16 Distribution of earthquakes occurred during January 1981 to March 1988 after The Research Group for Active Tectonics in Kyushu (1989).

may have relation to this depression). Furthermore, combination of these movements can produce northeast fracturing with right-lateral slip component, demonstrated by the Hinagu fault in the southwest Kyushu.

6. Conclusions

The three full-scene LANDSAT TM images of the Kyushu district, southwest Japan, were used to characterize local and regional fracture systems by combining the lineament data and DEM of 250 m spacing. The STA, which considers an illumination effect by semivariogram of the gray levels of image, successfully derived 77,893 lineaments from the images. 2,090 normal fault type and 3,238 reverse fault type fracture planes were interpreted to calculate strike and dip through the combination. The estimated fracture distributions were available to examine azimuthal relation between continuous fractures and principal veins, detect dangerous fractures for landslide, and reveal conjugate fracture pattern in a seismic zone. For the Hohi geothermal area in the middle Kyushu, the significant fractures trending northwest and north-northwest, which act as conduits for transport of hydrothermal fluids to the ground surface, could be identified and incorporated into numerical simulation for conjecturing hydrothermal fluid flows.

By classifying the estimated fracture planes according to the nine principal lithologic units in which they are distributed, local features regarding dominant azimuths that are common to the lithologic units in the southern part of Kyushu or the ones in the northern part were detected. The features may result from the difference in the history of tectonic stress fields be-

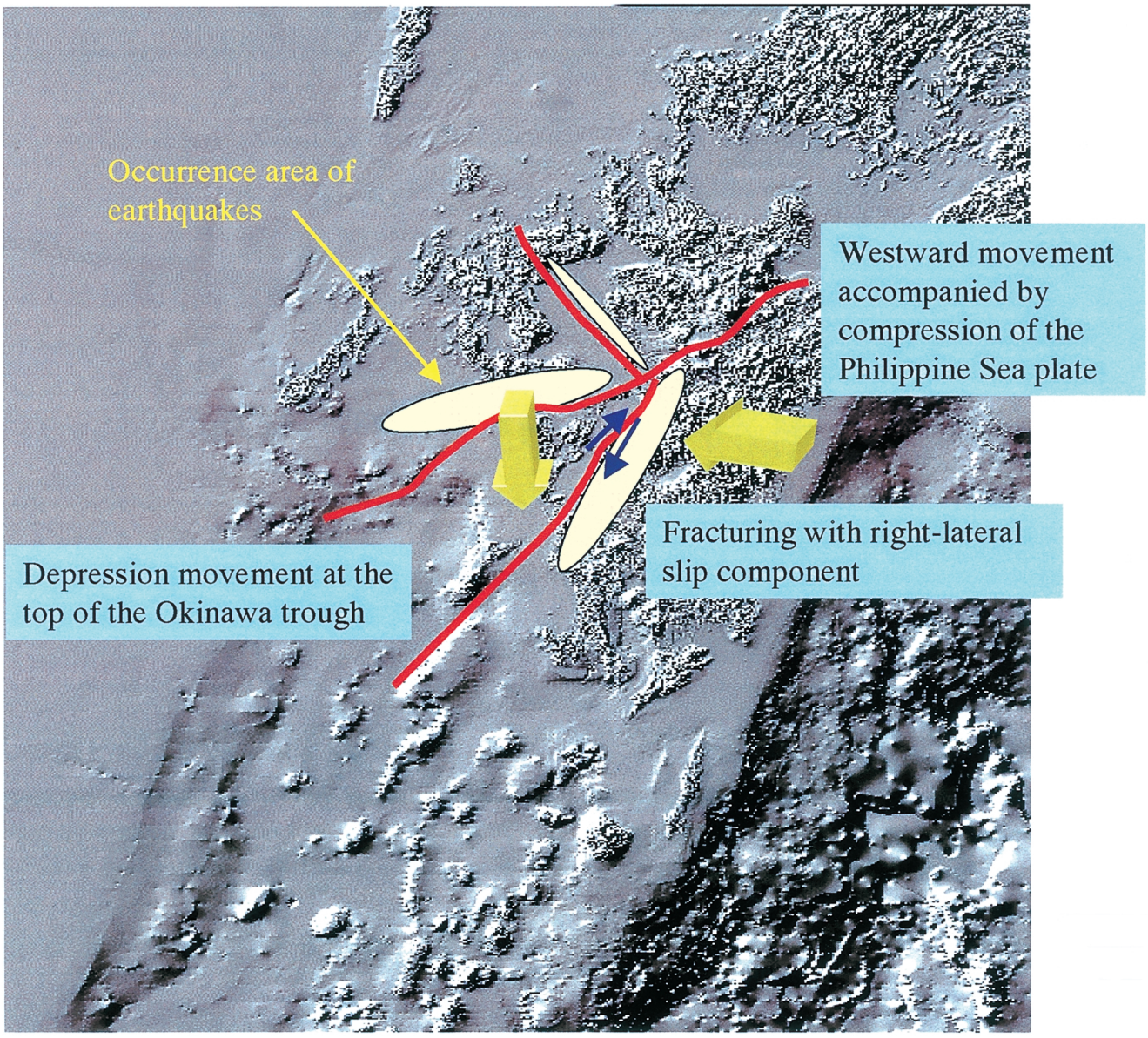

Fig. 17 A hypothesis on present tectonic model of Kyushu for configuring the fracture system, which consists of a westward movement of the southern Kyushu accompanied by the compression of the Philippine Sea plate, and a depression movement at the top of the Okinawa trough.

tween the two areas.

In addition, lineament analysis for the sea floor was conducted using the shaded DEM of 1 km mesh, produced by interpolating the sea-depth data. A combination of lineament maps of the land and the sea floor is useful to identify tectonically significant lineaments that are continuous over the two regions. We made a hypothesis on the present tectonic model of Kyushu considering the depression movement at the top of Okinawa trough and the westward movement of the Philippine Sea plate.

Consequently, the lineament analysis proposed by this study can contribute to understand many kinds of fracture-related phenomena that are important in resource exploration, disaster-prevention engineering, hydrogeolgy, and crustal deformation.

Acknowledgments: The authors wish to express their grateful thanks to Yuichi Ichikawa and Motoyasu Kusunose for improving the lineament extraction method and helping the data analysis. The LANDSAT satellite data we used in this paper partly bought through RESTEC (Remote Sensing Technology Center) for the aim of research. All the original data of LANDSAT are retained by the Government of United States of America and are supplied through Space Imaging EOSAT and NASDA (National Space Development Agency).

References

Adler, P.M. and Thovert, J.-F. (1999) *Fractures and Fracture Networks.* Kluwer Academic Publishers, 429 p.

Coward, M.P., Daltaban, T.S. and Johnson, H. (eds.) (1998) *Structural Geology in Reservoir Characterization.* Geological Society, London, Special Publications, 127 p.

David, M. (1977) *Geostatistical Ore Reserve Estimation.* Elsevier, 364 p.

Engelder, T. (1982) Is there a genetic relationship between selected regional joints and contemporary stress within the lithosphere of North America?. *Tectonics,* **1**, 161–177.

Geological Survey of Japan (1995) *Digital Geological Map,* G-1.

Koike, K., Nagano, S. and Ohmi, M. (1995) Lineament analysis of satellite images using a Segment Tracing Algorithm (STA). *Computers & Geosciences,* **21**, 1091–1104.

Koike, K., Nagano, S. and Kawaba, K. (1998) Construction and analysis of interpreted fracture planes through combination of satellite-image derived lineaments and digital elevation model data. *Computers & Geosciences,* **24**, 573–583.

Koike, K., Ichikawa, Y., Kouda, R., Ueki, T. and Gu, B. (1999) Estimation of fracture planes distribution pattern in southern Hyogo Earthquake area using satellite image and digital elevation model data. *Journal of the Remote Sensing Society of Japan,* **19**, 1–19 (in Japanese with English abstract).

Koike, K. and Ohmi, M. (1999) Preliminary study on construction and characterization of seafloor elevation model. *Geoinformatics,* **10**, 90–91 (in Japanese).

Koike, K., Tomita, S., Yoshinaga, T. and Ohmi, M. (2000) Fracture zone characterization in geothermal field using satellite image, fluid flow analysis, and radon prospecting : A case study of the Aso Caldera, southwest Japan. *Proc. 25th Workshop on Geothermal Reservoir Engineering,* Stanford University, CD-ROM press.

Koike, K. and Tomita, S. (2000) Three-dimensional modeling of geothermal systems using Curie point depth. *Abstracts of Stanford Geothermal Program 17th Annual Review Meeting,* 87–98.

Lippmann, M.J., Truesdell, A.H. and Gutiérrez Puente (1997) What will a 6 km deep well at Cerro Prieto find?. *Proc. 21st Workshop on Geothermal Reservoir Engineering,* Stanford University, 19–27.

MMIJ (The Mining and Materials processing Institute of Japan) (1989) *Gold Mines of Japan.* Part I. Kyushu district : MMIJ, Tokyo, 144 p. (in Japanese).

Nakazawa, T. (1997) Outline of the 1997 Izumi debris flow and its geologic setting. *Chishitsu News,* no. 517, 42–47 (in Japanese).

National Research Council (1996) *Rock Fractures and Fluid Flow, Contemporary Understanding and Applications.* National Academic Press, 551 p.

Rouleau, A. and Gale, J.E. (1985) Statistical characterization of the fracture system in the Stripa granite. Sweden, *Int. J. Rock Mech. Min. Sci. & Geomech. Abstr.,* **22**, 353–367.

Rowan, L.C. and Wetlaufer, P.H. (1981) Relation between regional lineament systems and structural zones in Nevada. *American Assoc. Petroleum Geologists Bull.,* **65**, 1414–1432.

Shiono, K., Wadatsumi, K. and Masumoto, S. (1987) Numerical determination of the optimal bedding plane. *Geological Data Processing,* no. 12, 299–328 (in Japanese with English abstract).

Tamanyu, S. (1985) Stratigraphy and geologic structures of the Hohi geothermal area, based mainly on the bore hole data. *Rept. Geol. Surv. Japan,* no. 264, 115–142 (in Japanese with English abstract).

The Research Group for Active Tectonics in Kyushu (1989) *Active Tectonics in Kyushu.* University of Tokyo Press, 553 p.

Urashima, Y., Ibaraki, K. and Suzuki, R. (1987) The Hishikari gold-silver deposit. *Gold Deposits and Geothermal Fields in Kyushu,* The Society of Mining Geologists of Japan, 27–38.

Received July 2, 2001
Accepted November 15, 2001

地形と地質データに重ね合わせた衛星画像リニアメントに基づく九州の断裂系の特徴抽出

小池克明・古宇田亮一・植木俊明

要　旨

主要なリニアメントは，鉱物資源や地熱資源を胚胎させる断層破砕帯と関連する場合が多い．したがって，陸域と海底の両方を対象としたリニアメント解析は，局所的・広域的な断裂系の特徴を広く理解するのに重要である．この理由から，線素追跡アルゴリズム（STA）と称するリニアメント自動抽出法，およびリニアメントデータと数値地形モデル（DEM）データとを組み合わせ，推定断裂面の走向・傾斜を算定するベクトル解析法を開発した．九州を解析対象地域に選び，LANDSAT TM バンド 4 データを用い，3 枚のフルシーン画像から 77,893 本のリニアメントを抽出した．高品位の浅熱水性鉱脈型金鉱床の周辺においては，連続性の良い推定断裂面の方位が主要鉱脈の方位と概ね対応し，鉱床胚胎と断裂系生成との関連が見出された．九州中部の豊肥地熱地域では，熱水が深部から地表へと上昇する際に通路となり得る重要な断裂が推定できた．さらに，水深データを補間することで 1 km 格子間隔の DEM を作成し，この陰影図を用いて海底地形のリニアメント解析を行った．陸域と海底のリニアメント図の組み合わせは，2 つの地域に連続する地質構造的に重要なリニアメントを見出し，断裂系の形成メカニズムの考察において有効である．